EarthArXiv Submission Coversheet

The following manuscript/dataset has been submitted to *Landslides* for review. The version here presented is a non-peer reviewed preprint submitted to EarthArXiv

Title:

Spatial and morphometric relationships of submarine landslides offshore west and southwest Iberia

Authors:

Davide Gamboa

Instituto Português do Mar e de Atmosfera – IPMA, I.P.; Rua C do Aeroporto, 1749-077 Lisbon, Portugal

davide.gamboa@ipma.pt

Twitter: @GambixPT

Rachid Omira

Instituto D. Luiz – IDL; Faculdade de Ciências da Universidade de Lisboa, Campo Grande, Edifício C8, Piso 3, 1749-016 Lisbon, Portugal

raomira@fc.ul.pt

Pedro Terrinha

Instituto Português do Mar e de Atmosfera – IPMA, I.P.; Rua C do Aeroporto, 1749-077 Lisbon, Portugal

pedro.terrinha@ipma.pt

Corresponding author:

Davide Gamboa – davide.gamboa@ipma.pt

Spatial and morphometric relationships of submarine landslides offshore west and southwest Iberia

Davide Gamboa[1*], Rachid Omira[1,2], Pedro Terrinha[1,2]

[1] Instituto Português do Mar e de Atmosfera – IPMA, I.P.; Rua C do Aeroporto, 1749-077 Lisbon, Portugal

[2] Instituto D. Luiz – IDL; Faculdade de Ciências da Universidade de Lisboa, Campo Grande, Edifício C8, Piso 3, 1749-016 Lisbon, Portugal

*corresponding author: Davide Gamboa (davide.gamboa@ipma.pt)

Abstract

Submarine landslides are ubiquitous geohazards in marine environments occurring at multiple scales. Increasing efforts have been made to catalogue and categorise submarine landslides in comprehensive databases, aiming to better understand their preconditioning and trigger factors. Using the recently compiled, open-access MAGICLAND dataset, we investigate the distribution and morphometric trends of submarine landslides observed in seven distinct geomorphologic domains offshore west and southwest Iberia. In the study area, the higher densities of submarine landslides occur on the proximal southwest margin, with higher frequency nearby earthquake epicentre clusters recorded in the area. Submarine canyons are another major location for slope collapses, with a prevalence for their mouth regions. However, relevant numbers occur within all domains with important relief, including distal regions hundreds of kilometres away from the foot of the continental slope. Landslide size range is inversely proportional to their spacing and frequency within each domain, and within the whole study area. Relevant positive correlations were obtained between the parameters analysed, but relationships between unidimensional parameters such as length and width exhibit the lower correlation coefficient. Correlations of 2D and 3D parameters such as area and volume provide better results, aligning with prior observations. The relationships obtained are, however, variable across domains and the correlation values are influenced by the seafloor geomorphology. This work brings new insights on submarine landslide distribution in the understudied west and southwest Iberian continental margin, complements previous inventories made for nearby regions, and provides valuable data with wider applications for submarine landslide databases.

Keyworks: Submarine landslides, Iberia Margin, morphometric relationships, morphological domains, geohazards, NE Atlantic

1. Introduction

Submarine mass movements are common occurrences on marine domains, from the shallow coasts to the deepest areas of the oceans (Hampton et al. 1996; Masson et al. 2006). Although outstanding massive deposits attract the attention for detailed studied, such as for example the Storegga Slide (Bryn et al. 2005; Micallef et al. 2008), the regions where ordinary landslides occur record geological evidence of hundreds or thousands of smaller-scale landslides (Chaytor et al. 2009; Casalbore et al. 2020), often overlooked due to poor data coverage or resolution. However, submarine landslides are a primary geohazard in marine environments and the extensive characterisation of their occurrence, at all scales and ages, on proximal and distal oceanic regions is crucial. Tsunamis generated from landslides on the flank of subaerial topography plunging into the sea (Siebert 1984; Ward and Day 2001; Bardet et al. 2003) or from large collapses on fully submerged morphologies (Harbitz et al. 2014; Omira et al. 2016) area a major concern. Moreover, seabed geotechnical installations and infrastructures such as submarine communication cables, pipelines, submarine observatories or any purpose-build platform are sensible to underwater mass movements (Pope et al. 2015; Clare et al. 2019). Recognising submarine landslide extents has further political implication as these are used to set international ZEE boundaries under the definition of the UN Convention on Law of the Sea (Mosher et al. 2016). It is thus crucial to understand the distribution patterns and morphometric trends of submarine landslides according to the regional setting in which they occur, with the aim to develop a solid knowledge on their causal mechanisms and resulting deposits (Camerlenghi et al. 2010; Moscardelli and Wood 2016; Clare et al. 2019).

An increasing number of efforts has been made to compile databases of submarine landslides aimed to better understand their distribution and morphometry on marine settings around the world (Clare et al. 2019). Regional compilations are available from the US Atlantic margin (ten Brink et al. 2009; Chaytor et al. 2009; Twichell et al. 2009), the Mediterranean Sea (Camerlenghi et al. 2010; Migeon et al. 2011; Urgeles and Camerlenghi 2013; Casalbore et al. 2020), the Spanish margins (León et al. 2020), Australia (Clarke et al. 2019) or New Zealand (Watson et al. 2020), to list a few examples. Global data compilations are also available to compare landslides on distinct continental margins of specific settings (Moscardelli and Wood 2016; ten Brink et al. 2016; Blahůt et al. 2019). However, extensive submarine landslide characterisation is still limited in many continental margins such as western and southwestern Iberia (Figure 1) and adequate characterisation depends on the quality of available data. This work is based on the MAGICLAND (MArine Geohazards InduCed by underwater LANDslides in the SW Iberian Margin) database (Gamboa and Omira 2021; Gamboa et al. 2021b), which compiled geomorphological data of 1552 morphological scars and submarine landslides offshore Iberia, to analyse their distribution and morphometry, and how these vary within seven offshore geomorphologic domains here established. Our results are important to understand the broad distribution of geohazards on the area, and aim to

contribute to global efforts to compile landslide information in different geological and oceanic settings.

2. Physiographic overview

Iberia is located on the Eurasian plate, just north of the African-Eurasia plate boundary at the easternmost termination of the Azores-Gibraltar Fracture Zone (Purdy 1975) (Figure 1). The modern physiographic features of the offshore West Iberian Margin (WIM) are determined by the main tectonic events that followed the breakup of Pangea, the Mesozoic rifting, the Atlantic seafloor spreading and the Cenozoic shortening and compressive reactivation of the Portuguese Margin (Alves et al. 2003; Terrinha et al. 2020) and interactions with long-lasting oceanic bottom currents (Hernandez-Molina et al. 2003)

2.1. Continental shelf and slope

The WIM west-dipping continental shelf and slope vary significantly in width, from less than 6 km to more than 70 km, along a 750-km-long stretch of coast parallel to the Mid Atlantic Ridge. To the north, the shelf is about 30-40 km wide, marked by a break at 160 m depth towards to a steep slope (circa 5º) and smoother continental rise totalling 100 km wide (Pinheiro et al. 1996; Alves et al. 2003). The Porto and Vigo Seamounts stand out as the most conspicuous features of the slope off north WIM (Vázquez et al. 2008) (Figure 1b and 2).

 Offshore central Portugal the shelf maximum width is up to 70 km, although narrowing intensely at the head of large Nazaré and Lisbon-Setúbal canyons. The slope, circa 50 km wide, is steep and widely incised by canyons and gullies (Mougenot et al. 1984; Alves et al. 2003). The Estremadura Spur is a major tectono-morphic feature where the continental slope gently dips westward at a constant gradient of 4º from 300 to 3000 m depth (Badagola 2008). To the north and south of the spur the shelf and slope show clear marks of vertical erosion and regional slope gradients reach up to 13º (Alves et al. 2003; Terrinha et al. 2020).

The southwest margin is limited by the Setúbal and São Vicente Canyons (Figure 1b). It exhibits a gentler and wider continental slope, with a less clear transition from a narrow shelf not exceeding 20 km of width (Pinheiro et al. 1996). Steep gradients in this margin segment only occur close to seamounts resultant from Alpine compression, fault scarps and areas of localised deformation (Mougenot et al. 1984; Terrinha et al. 2003).

The continental shelf of the south margin varies in width from ~5 km to ~40km and has slope domain with steeper gradients closer to the shelf, shifting to a lower gradient mid-slope terrace covered by Pliocene-Quarternary contourite drifts (Marchés et al. 2007; Ducassou et al. 2016). The south SWIM margin comprehends various major morphologic and drainage features, such as the Portimão canyon (~70 km long) and the margin parallel submarine valleys that exceed 200 km in length, the Cadiz and D. Carlos valleys (Hernandez-Molina et al. 2003; Terrinha et al. 2009)

2.2. Canyons and deep-marine features

The west and southwest shelf and slope are incised by several submarine canyons, with relevance for the Nazaré, Cascais-Lisboa-Setúbal system and the São Vicente canyons (Figure 1b). Their thalwegs typically exceed 1500 to 2000 m, and the incision paths generally align with major fault structures delimiting tectonic blocks (Montenat, et al. 1998), some of which are seismically active as the São Vicente canyon (Silva et al. 2017).

Off the west and southwest continental slope and rise, major bathymetric features rise hundreds to thousands of metres from the deep seabed, delimiting the major abyssal plains (Figure 1b). To the north, the Galicia Bank is a main unit consisting of remnant rift structures (Montenat, et al. 1998). Adjacent to the Estremadura Spur, the elongated Tore Seamountain extends westward for about 240 km (Figure 1b), formed by coalesced ridges and seamounts that surround an inner asymmetric depression that, at its maximum, is deeper than the surrounding Iberia and Tagus Abyssal Plains (Roque et al. 2009; Terrinha et al. 2019). This feature is the northernmost termination of the Madeira-Tore Rise, which is punctuated along its length by numerous volcanic peaks (Merle et al. 2018).

To the southwest, east-west trending seamount chains border the abyssal plains, namely the Gorringe-Josephine chain separating the Tagus and Horseshoe Abyssal Plains, and the Coral Patch Ridge – Lion Seamount separating the Horseshoe and Seine Abyssal Plains (Figure 1b). The seamounts have variable genesis derived from volcanic and/or tectonic processes (Girardeau et al. 1998; Gamboa et al. 2021a), often associated with reactivated rift structures (Tortella et al. 1997; Terrinha et al. 2019). Large mass-failures occurred on the seamount flanks (Lo Iacono et al. 2012; Omira et al. 2016; Gamboa et al. 2021a), but widespread collapses have been identified at various scales (Gamboa et al. 2021b).

The southern offshore morphology results from combined tecto-stratigraphic, creating features as the Portimão-Guadalquivir Bank, a pop-up block in-inherited from the Mesozoic rifting (Gràcia et al. 2003), or the Guadalquivir ridge, associated with salt and mud diapirism (Maldonado et al. 1999). Evidence of numerous mass-wasting events is present on the flanks of these elongated banks (Camerlenghi et al. 2010; Silva et al. 2020). The Accretionary Wedge of the Gulf of Cadiz is a main morpho-tectonic feature originated by west-verging thrusts where instability due to fault reactivation, diapirism and fluid escape processes is common (Pinheiro et al. 2003; Medialdea et al. 2004; Terrinha et al. 2009). These, in conjunction with the dense Mediterranean Outflow Water (MOW) dynamics, result in variable and complex morphologies (Hernandez-Molina et al. 2006; García et al. 2009; Duarte et al. 2010) (Figure 1b).

3. Methodology

The mapping of scars and landslide features was based on the 2018 version of the EMODnet DTM for European seas covering the West and Southwest Iberian margin

(EMODnet Bathymetry Consortium, 2018) (Figure 2). The grid has a general 115 x 115 m resolution, complemented by higher resolution areas. Mapping of the landslides' morphological features followed, as possible, the criteria and nomenclature established by Clare et al (2019) for direct measurements, complemented by additional calculated parameters. Detailed descriptions of the methodology workflow and processes used to acquire the submarine landslide dataset are available in Gamboa et al. (2021b, in press), and the data is available in Gamboa and Omira (2021). As noted in Gamboa et al. (2021b), two sets of measurements were taken for certain parameters where one derived from a planimetric (2D) perspective (e.g., L_t in the database) and a second one derived from the projection of the line path or areas over a 3D surface with a slope gradient (e.g., L_{t-r}). As the latter measurements account for the seafloor morphology and gradients, all data presented in this work regarding the length, width and area parameters (and derived calculations) correspond to the "realistic" values obtained.

The statistical analysis undertaken was applied to the full dataset samples and to seven subsets representative of different geomorphologic offshore domains (Figure 2). Spatial statistics analysis includes Kernel Density (KD) and nearest neighbour calculations (Figures 3 and 4). The KD calculates a magnitude-per-unit area from the input features to fit a tapered surface. Here, we used the line feature delimiting the landslides as input. The line KD was adapted from the quartic kernel function for point densities (Silverman 1986), being greater at the line and zero at the limit of the radius distance, which was set at 30 km. The nearest neighbour tests the clustering or overdispersion of points. It calculates the distance between the closest pairs of point, and compares the observed pair values with those expected from randomly place points (Davis 2002). The input point was the landslide XY reference, located at a mid-width position near the scar. The nearest neighbour produces a Z value, where negative or positive values respectively indicate clustering or evenness/overdispersion. The expected-to-observed distance ratio R is also calculated, where 0<R<1 indicates full clustering and no distance between points, R=1 indicates random distributions, and R>1 overdispersion (Davis 2002). Directional representation of the landslide flow azimuth was made using rose diagram plots. Power-law scale relationships were established to compare pairings of morphometric parameters, represented in the form of:

$$Y = k. X^b \qquad (1)$$

The power-law relationships were used to evaluate the correlation between parameters for the full sample and the sub-samples of each domain, and are plotted alongside their Coefficient of Determination, or R^2. Pearson´s Correlation Coefficients were calculated to assess the linear correlation between variables.

4. Submarine landslide distribution

The 1552 submarine landslides in the database were grouped into subsets for seven geomorphological domains (Figures 2), namely: 1) Submarine Canyons, which include the broadly E-W oriented Nazaré, Cascais, Lisboa and Setúbal canyons, and the S-SW

oriented S. Vicente, Lagos and Portimão Canyons on the southern slope; 2) Estremadura Spur Domain; 3) broader Gulf of Cadiz (GoC) Domain, comprising irregular morphologies within the GoC accretionary wedge and slope; 4) GoC Banks Domain, an elongated region immediately adjacent to the southern of the slope which includes east-west trending channels flanking large banks; 5) a general Distal Domain, comprising numerous submarine ridges and seamounts of variable size and shape on the distal western regions of the study area, including the Madeira-Tore Rise; 6) Seamount Chains Domain, including the major submarine seamounts rising up to 4000 m from the abyssal plains; 7) Continental Slope Domain, which covers the extent of Portugal´s continental slope, except where intersected by Domains 1 and 2.

4.1. Kernel density

The submarine landslide distribution is non-uniform, occurring on and along specific areas of the offshore ruled by the presence of submarine relief and with prevalence on proximal areas, as illustrated by the kernel density map in Figure 3. The blank areas within the map represent KD values of zero.

From the areas with KD values exceeding 0.2, the higher values (up to 0.35) are located on the southern margin within an area over 100 km long that crosses portions of Domains 1, 3, 4 and 7 (Figures 2 and 3). Other higher KD clusters occur to the west overlying both flanks of the Gorringe Bank. Along the WIM, the higher density patches occur within submarine canyons (Domain 1). The major cluster, with KD values over 0.3, is a result of the proximity of three canyons (Setubal, Lisboa and Cascais) and reflects the high number of slope failures within them. Further north, and across the Estremadura Spur, the higher density patch (KD >2) is associated with the Nazaré canyon. In both canyon-related clusters, the highest density values coincide with the canyon mouth area and transition to less confined morphologies.

Other landslide clusters dispersed in the study area have KD values generally around 0.15 or below. These distribute in Domains 2, 5 and 6 where seamounts and ridges of all sizes prevail (Figures 2 and 3), with sub-circular to elongated KD patches inherited from the geomorphology of the submarine relief. Within the Gulf of Cadiz (Domain 3), the major cluster observed towards the SE of the study area is fairly wide (Figure 3), contrasting with the clusters over seamounts, reflecting a morphology within the accretionary wedge marked by numerous smaller landslides (Figure 2). However, towards the western limit of Domain 3 the smaller subcircular KD patterns represent landslides flanking small diapirs and ridges. On the continental slope (Domain 7), patches of low-density areas occur between the main canyon areas, particularly within the SWIM. Domain 7 also includes the Porto seamount cluster, located within the broader slope limits (Figures 2 and 3).

4.2. Nearest-neighbour analysis

The nearest neighbour analyses were undertaken to quantify the distance between landslide occurrences within each individualised domain (Figure 4), and show the frequency of observed distances alongside the expected nearest neighbour model. The table on the lower right of Figure 4 summarises, for each domain, the number of points, mean and expected distances, Z statistic (standard normal variate), the probability of a random distribution and if there is statistically significant point clustering.

With the exception of the Estremadura Spur (Domain 2), all domains show similar trends for the nearest neighbour results. High frequencies are recorded for the lower quarter of distance values, with the observed value being at least two to three time their expect distance model. The mean distance for each domain, about 50% to 60% of the expected value, also reflects this trend. The exception is in Domain 4 where the mean value is 80% of the expected distance. The nearest neighbour results also show that, except for Domain 2, there is statistically-supported indicators for landslide clustering in all domains (Figure 4). For Domain 2, the observed frequencies for distance show a proximity for the expected curve, and the mean value is about 90% of the expected one. The Z and R results for Domain 2 are also closer to the reference values for random distributions, suggesting a tendency towards an evenness of point distribution rather than high clustering trends.

4.3 Landslide flow direction

The rose diagrams in Figure 5 illustrate the landslide flow azimuth within each domain. The orientations are, as expected, sub-perpendicular to the major trends of the morphological features within each domain. In Domain 1, the broad N or S-directed flows derive from the predominant E-W and SE orientation of the canyons on the margin (Figure 2). The diagram shows a fairly wide range of orientations within each quadrant as a result of the slightly sinuous canyon paths. On the Estremadura Spur (Domain 2), there are flows towards all quadrants around this radial morphological feature, except in the gap between N30 and N90 directed towards the continental shelf (Figure 2). On the continental slope (Domain 7), which the canyons incise, the landslide flow ranges between SE to NW orientations, expected from the margin orientation. The high frequency of NE-direct failures within Domain 7 is due to localised topography within this broader area such as, among others, the Porto seamount or tectonic relief on the SWIM (Figure 2).

Within the broader GoC, distinct trends are observed for its two domains (Figure 5). For the near-slope banks and wider channels in Domains 4, there is a clear distribution of flows directed towards the northern or southern quadrants, with extremely scarce occurrences towards east or west. This represents the mass-failures along both flanks of the elongated banks. In Domain 3, which includes the large accretionary wedge and other tectonic morphologies, the predominance of westward-directed flows coincides with the general slope gradient on the same direction.

The ridges and seamounts on Domains 5 and 6 display several landslide orientations covering the whole range of azimuths. However, some main trends are discernible, again influenced by the major bathymetric trends. On Domain 5, there are clear higher frequencies towards the West and East, strongly influenced by collapses on the numerous N-S small ridges located on the distal portions of the study area (Figures 2 and 3). The NNE component is related to morphologies further south. Regarding Domain 6, the broad range relates to the variable orientations of the very large, elongated seamounts and the slight orientation shifts along the major chain they are part of (Figure 2). The higher frequency towards NNE orientations is in part influenced by numerous slope failures in the flank, and in sub-basins, of the complex Tore Mountain morphology.

5. Morphometry of submarine landslides

Figure 6 shows a selection of ten morphometric parameters typically used to characterise submarine landslides. Data shows that average length and width values do not drastically change across the domains, ranging between 2.5 to 4 km. The ranges of values for these parameters are representative of the distinct magnitude of mass-failure across domains, with the larger and wider ones on Domains 5 and 6 also exhibiting the largest height range and deeper depths of occurrence. The smaller length and width values are recorded for landslides on Domains 3 and 4, being also the ones with overall lower height. More representative of the morphometric variations across domains are area and volume. Even with a log scale representation, the dimensional ranges are striking. The larger landslide area and volume occur on Domains 5 and 6, and the smaller ranges are observed on Domains 3 and 4. The remaining Domains 1, 2 and 7 (i.e., Canyons, Estremadura Spur and Continental Slope) show fairly similar ranges of morphometric parameter values between them, as well as similar heights and scar depths. This is mostly due to the identical geomorphologic character of the domains in which they occur.

The aspect ratio of landslides is frequently used to compare and contrast morphologies at different locations. Here, we use the length/width ratio (L/W), where L/W ratios >1 represent elongate landslides and ratios <1 represent transverse ones (sensu Gamboa et al. 2019). Values of L/W ratios over 1 and up to 4 are observed in all domains, expected for "classic" elongated landslide geometries and representative of the largest deposit identified. However, out of the 1552 features, 945 (61%) have L/W <1, and from these 249 (16% of the total) show ratios below or equal to 0.5, i.e., the landslide width is at least the double of its length. Most of these occur on Domains 3, 5 and 6, although also present in all others. Notwithstanding, numerous transverse slides were observed and this also mirrors limitations derived from the Digital Elevation Model (DEM) mapping and the lack of subsurface data for an adequate assessment of buried landslide portions.

Morphometric information of the scar length and sinuosity is also presented. The vast majority of scars has less than 10 km, but numerous outlier points illustrate the presence

of quite extensive ones. The largest scar lengths are recorded on Domain 6, where landslides on the flanks of hundreds to thousands of metres high seamounts show several scars between 20 and 60 km long. Noteworthy scar lengths in excess of 10 km are also observed on Domains 1 and 7 which, despite associated with some of the lower depths, exhibit very steep, high slopes. The purpose to represent scar sinuosity was to document the variable shape of these features. Minimum values of 1 represent (quasi-)linear scars, whereas values further away from this indicate bell or U-shaped scars (typical of landslides) that may include long lateral wall segments. Unlike observations for other properties, the scar sinuosity shows approximately similar patterns across all geomorphological domains. Worth noting is that the boxplot for Domain 5 shows the narrowest inter-quartile range, indicating a high frequency of linear scars, possibly associated with landslides on the flanks of elongated ridges in the distal areas.

6. Scale relationships of morphometric parameters

Scale relationships have been analysed between distinct morphometric parameters, primarily using the power-law in Equation 1.

The first example focuses on the relationship between the measurements of a parameter based on planimetric perspectives and its value on a three-dimensional perspective affected by a slope gradient (Figure 7). Length (L_t and L_{t-r}) and area (A_t and A_{t-r}) are used to exemplify this objective. The ratio between both length measurements is clearly influenced by the slope gradient measured along the path of the length vector (Figure 7a). Lower slope gradients lead to a closer proximity between the two- and three-dimensional measurements. At slope gradients of 5 to 10 degrees, a range widely observed in our examples (Figure 6g), results indicate that L_t measurements can be 10% to 15% lower than the realistic downslope length (Figure 7a). Towards the steeper gradients recorded, this difference between measurements can be close to 40%. Unlike the other examples, the relationship between length ratios and slope gradient fits adequately with an exponential trend, with very high correlation values (R^2=0.97). This trend excludes the two outlier points with length ratios below 60. Scale relationships between length measurements were established (Figure 7b), with nearly perfect fits for the power-law trends. As the b exponential value is very close to 1, based on the obtained K value the L_{t-r} value can be generally considered as 16% higher than L_t measurements derived from planimetric perspectives. Similar outcomes were obtained for the comparison between A_t and A_{t-r} (Figure 7c). With exponential values of 1, the K value of 1.026 can be considered as a direct scaling value between A_t and A_{t-r}, with the later being about 3% larger.

The power-law relationships between length, width, area and volume, four of the most relevant parameters in landslide morphometrics, are summarised in Figure 8. The relationships on the scatter plots apply for the full sample, irrespective of the domains in which the landslides occur. Volume-based relationships used a smaller sample with 1450 features which excludes values lower than 0.01 km^3.

The length-width relationships generally show the lower correlations. Graphically, this is expressed by the marked scatter of the data from the trend line. Even towards the higher values the scatter range persists, despite the lower frequency of observations. The Pearson correlation mimic this, with some of the lower values being recorded for the whole sample and in the different domains as well comparatively to other parameter pairings. Other parameter relationships that do not yield optimal R^2 values are length or width relationships with volume, with coefficients of 0.72 and 0.63, respectively. Likewise, this lower fit is reflected on the Pearson correlation values.

Improved relationships were obtained between the area and remaining parameters. Area-length power-law relationships yield a $R^2 = 0.85$, while area-width and area-volume both show $R^2 = 0.80$. Plots for these relationships show a tighter dispersion of the data from the trend line, with this being fairly uniform for the length-area and width-area ones. However, volume-area relationships show higher scatter from the trendline for values below 50 km^2, where there is a higher mix of features from all domains. Above this value, the scatter is tighter and the data mostly corresponds to Domains 5 and 6. The Pearson correlation is improved as well, with the highest values observed for Domains 5 and 6 as well.

6.1. Domain relationships

As relationships variations occur between the distinct domains, individual power-law relationships were established for each one (Figure 9). This allows a better understanding of what relationships best fit specific scenarios, and how much domain-specific relationships deviate from the unsorted sample.

The area-volume relationships for individualised domains shows marked variations, with R^2 values ranging between 0.527 and 0.854 (Figure 9). The best fits are observed for Domains 5 and 6, which also show the larger data ranges. Domains 2, 3 and 4 have the lower correlation values as well as the shortest data ranges for both area and volume. This may be due to the lower frequency of features and the scattered point patterns compromise the adequate relationship. Plotting the seven trendlines together allows a direct comparison of the relationships between domains (lower right panel in Figure 9). Although the steeper lines correspond to the domains with the higher correlation between area and volume, this aspect cannot be considered as an unequivocal diagnostic as the lower gradient lines do not necessarily correspond to the lower correlation values (e.g., Domain 2 vs Domain 3).

Comparisons of length-area relationships (Figure 10a) show good correlations for all domains. The lower R^2, of 0.7, is obtained for Domain 4, but for all others this is at least of 0.8. Similar to the observations for the full sample, Domains 5 and 6 have the higher length-area correlation with $R^2 = 0.9$. Despite small variations, all the power-law curves are fairly close and show similar slopes. However, the same deductions cannot be made for the length-width relationships (Figure 10b). If this relationship pair has some of the lower correlations for the full sample (Figure 8), the analysis breakdown for the distinct

domains further highlights the disparity. The higher $R^2=0.5$ is, as for other parameters, observed for the distal offshore domains, but values as low as 0.2 were obtained for Domains 3 and 7. The compiled trend lines also show a higher variability of their slope and a more erratic distribution, illustrating the higher variability of length-width relationships across geomorphologic domains.

6.2. Relationships between landslide evacuation and deposit sectors

A key objective in submarine landslide studies is to understand the preservation of mass by estimating the balance between the evacuated strata and the resulting deposit. From the full sample, 374 landslide instances (24% of the total) presented an associated deposit on the seafloor morphology. The relationship between the morphometry of the evacuation and deposition sections of the landslides have been analysed for the full sample and for each domain (Figure 11 and 12). Landslide deposits from Domain 2 (the Estremadura Spur) were excluded as only two features were identified. The relationships for the length and the area of the evacuation and deposit sections are presented, but additional parameters have been acquired (Gamboa and Omira 2021; Gamboa et al. 2021b).

The relationship between the deposit (L_D) and evacuation (L_{EV}) length shows limited correlation for the full sample, with R^2 values of 0.54 (Figure 11). However, *k* values of 2 and the plot data suggest that, at least for the denser point distributions, the length of the deposit can be approximately double the length of the evacuation sector. As for the individualised domains, the relationship trends are variable. On Domains 1, 5 and 6 the *k* values exceed 2, and several points fit in landslide deposit lengths as being twice the one of the evacuation sections. However, the variability of the R^2 values for these domains indicates a poor applicability for these relationships, with best but limited results being obtained for Domain 5 ($R^2=0.66$). The *k* value on the remaining domains varies between 1.56 and 1.66, but yet again the R^2 is very variable and indicative of low correlations, with values as low as 0.07 observed for Domain 3.

The relationship between the areas of the deposit and evacuation sections shows drastically different correlations (Figure 12). For the full sample, the $R^2 = 0.86$ is fairly high and suggests a good correlation between the evacuation and deposit areas. The *k* value of 1.45 and exponential values near 1 obtained from the power-law indicate that, in general, the area covered by the deposit tends to be 50% larger than the evacuation area. The area scale relationships obtained for the individualised domains shows similar trends, with generally good R^2 values above 0.7. The highest value is recorded for Domain 5 ($R^2=0.88$), while Domain 3 shows a markedly lower value of $R^2=0.46$ compared to all others.

7. Discussion

7.1. Submarine landslide distribution and morphometry

The occurrence of submarine landslides is the result of a set of longer-term preconditioning factors, with failure being awarded to a trigger event associated with the regional geodynamic setting (Lee 2009; Clare et al. 2019; León et al. 2020). The primary factor to consider for submarine landslide hazards is the bathymetric character of the area and associated slope gradients. Offshore western Iberia, submarine landslides have been, expectedly, recorded on every morphological domain established, except for the flat abyssal plains (Figures 2 and 3). The highest frequency of events is registered on the SWIM, with a major cluster on the south margin that includes submarine canyons, the Gulf of Cadiz banks, and nearby seamounts, with relevance for the Gorringe Bank. Given that major earthquake epicentre clusters are coincident with the higher kernel density of landslides (Figure 3), the data aligns with the consensus that the intense tectonic activity associated with fault activity on the Gulf of Cadiz is a main driver for mass-failures on the margin (Terrinha et al. 2003; Silva et al. 2017; Collico et al. 2020). Another major locus for landslide occurrence is within the submarine canyons. Canyon flank collapses can be in part associated with seismic activity, as several epicentres were registered near the canyon head areas (Figure 3). However, canyon flank undercut by sedimentary flows is probably a more relevant inducer for their wall collapses and often leads to an increase of failure frequency towards the canyon mouth (Casalbore et al. 2020), as observed in our examples (Figure 3).

The location of the studied landslides aligns with broad-scale landslide susceptibility studies made for the study area. Using the same base EMODnet DEM, Innocenti et al. (2021) estimated a medium to high susceptibility for landslides to occur as a response to the slope value. Although the results may lack accuracy for exact landslide occurrence, they align with our results as the higher susceptibility locations are generally coincident with the higher landslide density hotspots (Figure 2 and 3). These also correspond to any steeper areas of the continental slope, submarine canyons or seamounts. The major exception rests on the broader Gulf of Cadiz (Domain 3), namely within the rugged morphology over the accretionary complex. Although numerous small-scale collapses are observed, this area presented a low to moderate susceptibility modelled by Innocenti et al. (2021), which points to a control other than the slope gradient. Given the geological characteristics of Domain 3, likely preconditioning and trigger factors involved the accretionary wedge thrust tectonics and the influence of erosive bottom currents driven by the Mediterranean Outflow Water (MOW). The latter process also influences slope failures within Domain 4, as sediment remobilisation and slope undercut by MOW contour currents favour instability events on the GoC banks and valleys (García et al. 2009; Hernández-Molina et al. 2016). An earthquake-induced landslide susceptibility study for the SWIM by Collico et al. (2020), coincident with most of the southern half of our study area, provided similar results. On this, the steeper morphologies present yet again the highest probability of failure, coincident with the locations with higher KD values (Figure 3). In addition, Collico et al. (2020) show a moderate to high probability for earthquake-triggered failures to occur within the higher density area in Domain 3 (Figure 2), thus strengthening the tectonic influence in here,

but it was not clear if the model considered faults within the accretionary wedge or just major ones to the NW.

The spatial distribution and morphometric parameters of the submarine landslides are clearly influenced by the geomorphology of the domain in which they occur. Landslides on or close to the continental slope (Domains 1, 2, 3, 4, and 7) show smaller distances between scar locations, with the bulk of occurrences being about 4 km to 5 km, while on domains with seamounts the higher frequency of recorded spacing reaches about 10 km (Figure 4). The landslide spacing is proportional to their size as the domains of higher nearest neighbour results, namely 5 and 6 (Figure 4), show the largest areas, volume, length and width (Figure 6). Observations in other study areas have raised the point that the size of a given landslide may be overestimated if the morphological record on the DEMs is a result of coalesced scars from multiple, close events (Casalbore et al. 2020). This has been observed in all domains covered in this study, with the respective landslides being marked as multi-scar features (see Gamboa and Omira 2021). However, the sheer difference in landslide size scale between domains supports the premise that this primarily depends on their location rather than coalescing scars. On an additional note, morphology must also be considered for morphometric measurements as the effect of slope steepness will increase any dimensional trends obtained from map perspectives (Figure 7).

A main objective to determine power-law relationships between parameters is not only to obtain predictive trends but also to compare them to submarine landslide datasets using similar methods (Chaytor et al. 2009; Moscardelli and Wood 2016; Blahůt et al. 2019). This attempt of standardization is key for a closer comparison between datasets of different parts of the world compiled by different interpreters (Clare et al. 2019). One application relates to the submarine landslide classification scheme into detached or attached events (Moscardelli and Wood 2008, 2016), primarily established from the geodynamic setting they occur but with strong links to the scale of the mass-failures. The features here studied fit into the detached classification. However, several examples on both seamounts and continental slopes do exceed the morphometric ranges defined in Moscardelli and Wood (2016), further confirming that the size alone cannot be a diagnostic for classification (Gamboa et al. 2019). The parameter relationships are aimed to provide a near-predictive tool, thus pairs with higher correlation values should provide best results. Our results indicate that parameter relationships involving the area provide closer relationships, particularly area-volume and area-length (Figure 8, 9 and 10a), a pattern also observed in other landslide inventory studies (ten Brink et al. 2009; Moscardelli and Wood 2016; Blahůt et al. 2019; ten Brink and Geist 2021). The scale relationships between 2D and 3D measurements for length and area also support this (Figure 7). Landslide areas calculated from a 3D surface were only about 3% larger than those mapped on 2D, whereas for the length values this was about 16%. These fits are,

nonetheless, influenced by the morphology and geodynamic setting, as shown by the variability of R^2 across domains (Figure 9).

Length-width relationships consistently show the lower correlation (Figure 8 and 10b), likely a limitation of the unidimensional nature of these parameters to represent the 3D variability on landslides. Nevertheless, the use of the L/W ratio (or W/L, often used as well) as an indicator of the landslide general shape can also provide clues on the style of failure and remobilisation dynamics (Gamboa and Alves 2016; Gamboa et al. 2019; León et al. 2020). On typical landslide models, L/W ratios of 1 and above are expected as a result of a runout longer than the width. However, detached submarine landslides can frequently show ratios lower than 1, especially when associated with elongated, steep topography (Gamboa and Alves 2016). Values below 1 are recorded in all studies domains but domains 3 and 5 show the lowest averages (Figure 6h), indicating a relevant proportion of transverse landslides. Transverse slides fit with the low scar sinuosity values observed on Domain 5 (Figure 6j) and relate to numerous elongated ridges occurring there (Figure 1), in a similar trend to landslides adjacent to oceanic ridges on the Spanish ZEE (León et al. 2020). However, the number of landslides with L/W ratio inferior to 1 (60% of the sample) is likely overestimated due to limitations of the data used. As only a bathymetric DEM was used, it is possible that the true length of identified landslides is higher if their associated deposit is fully or partially buried, thus with limited or not expression on the seafloor. For this same reason, the number of interpreted landslide deposits and their exact length may be under-represented, a limitation that can only be overcome if subsurface data is available. The absence of deposits may also be due to the full disaggregation of the flow or posterior deposit removal (McAdoo and Watts 2004; Casalbore et al. 2020), thus skewering the sample towards lower ratios restricted to the evacuation area. Such remobilisation or reworking of the deposit is more likely to occur in areas with frequent turbiditic or contour current activity (Arzola et al. 2008; Stow et al. 2013; Miramontes et al. 2018; Casalbore et al. 2020) such as the submarine canyons, continental slope and areas of the Gulf of Cadiz affected by bottom currents.

7.2. Database applications and limitations

The MAGICLAND dataset derived from the need of thoroughly compiling submarine landslide evidences offshore west and southwest Iberia. Studies of specific large landslides (Omira et al. 2016; Gamboa et al. 2021a) or assessments of limited areas (Camerlenghi et al. 2010) of this margin have been made, but not to this areal extent or scales of analysis. Our results serve a two-fold objective. First, the provision of a data of value for wide-coverage databases of submarine landslide morphometry, immediately complimentary of landslide databases on the Spanish EEZ (León et al. 2020) and relevant for broader global scale objectives (Clare et al. 2019). Second, to pinpoint bathymetric features or areas of occurrence of large landslides that can have high tsunamigenic potential, especially ones on flanks of large seamounts (Harbitz et al. 2014; Omira et al. 2016). As mentioned, the sole use of DEM data presents limitations for the full

characterisation of the landslides and their flow dynamics or preservation potential as no subsurface data can be provided, and absolute runout distances and paths can be underestimated. However, it retains its value for tsunamigenic analyses as a key parameter is the evaluation of the quickly evacuated rock volume within the scar area and its disturbance on the water column.

As pointed for early interactions of databases, there are still knowledge gaps that can be filled as additional data becomes available (Blahůt et al. 2019; Collico et al. 2020). The data does show a skewness of analysis towards the southwest margin, driven by its inherent higher hazard potential and the improved data resolution. Future versions of this database aim to integrate subsurface information as well no only to complement the data collected but also investigate buried (young?) landslides on proximal high sedimentation environments at the canyon-delta transitions. It is also aimed to include still unmapped landslides, especially towards the northern regions of the WIM. The open availability of the dataset allows for further contributions from the research community that either complement the data or reuse it for complimentary parameter analysis.

8. Conclusions

The open-access MAGICLAND database was used to characterise the distribution and morphometric relationships of submarine landslides offshore west and southwest Iberia. The sample of 1552 features were subdivided into seven geomorphological offshore Domains. Results show that the higher densities of submarine landslides occur on the tectonically active Southwestern Iberian Margin, in areas coincident with numerous earthquake epicentre clusters, and within submarine canyons where numerous collapses occur on their flanks. Nevertheless, submarine landslides were widely identified on the flanks of bathymetric features in all domains, resulting in statistically significant clustered distributions. Positive Pearson correlation coefficients were obtained for correlations between length, width, area and volume, with relevance for area-volume pairings. Power-law relationships for the latter also show higher correlations for both the full sample and the domains subsamples. In contrast, length-width relationships tend to show the lower correlations. Despite the correlation variability observed, the distal domains consistently show the highest values while the domain within the Gulf of Cadiz presented the lower ones, indicating that submarine settings with higher geodynamic complexity can lead to higher variability of landslide morphology.

Our results align with similar analyses applied to other submarine landslide databases, indicating that unidimensional parameters are poorer predictive tools to estimate submarine landslide morphologies compared to 2D and 3D ones. Despite data-inherent limitations, results are valuable to understand the distribution and magnitude of submarine landslides and associated hazard potential offshore Iberia. Of particular interest was the identification of higher magnitude landslide locations, predominantly on the flanks of seamounts and ridges, to estimate their evacuation volumes and

tsunamigenic potential. Future, improved versions of the MAGICLAND will integrate subsurface data and/or higher resolution bathymetric grids as well as geotechnical properties of the substrate as they become available. Its open-source nature also allows further improvement, sharing and integration by the research community.

References

Alves TM, Gawthorpe RL, Hunt DW, Monteiro JH (2003) Cenozoic tectono-sedimentary evolution of the western Iberian margin. Marine Geology 195:75–108. https://doi.org/10.1016/S0025-3227(02)00683-7

Arzola RG, Wynn RB, Lastras G, et al (2008) Sedimentary features and processes in the Nazaré and Setúbal submarine canyons, west Iberian margin. Marine Geology 250:64–88

Badagola APL (2008) Evolução morfo-tectónica da plataforma continental do Esporão da Estremadura. Msc, University of Lisbon

Bardet J-P, Synolakis CE, Davies HL, et al (2003) Landslide tsunamis: Recent findings and research directions. In: Landslide tsunamis: recent findings and research directions. Springer, pp 1793–1809

Blahůt J, Balek J, Klimeš J, et al (2019) A comprehensive global database of giant landslides on volcanic islands. Landslides 16:2045–2052

Bryn P, Berg K, Forsberg CF, et al (2005) Explaining the Storegga Slide. Marine and Petroleum Geology 22:11–19. http://dx.doi.org/10.1016/j.marpetgeo.2004.12.003

Camerlenghi A, Urgeles R, Fantoni L (2010) A Database on submarine landslides of the Mediterranean Sea. In: Mosher DC, Shipp RC, Moscardelli L, et al. (eds) Submarine Mass Movements and Their Consequences. Springer, pp 503–513

Casalbore D, Clementucci R, Bosman A, et al (2020) Widespread mass-wasting processes off NE Sicily (Italy): insights from morpho-bathymetric analysis. In: Georgiopoulou A, Amy L, Benetti S, et al. (eds) Geological Society, London, Special Publications. Geological Society, London, Special Publications, 500, pp 393–403

Chaytor JD, ten Brink US, Solow AR, Andrews BD (2009) Size distribution of submarine landslides along the U.S. Atlantic margin. Marine Geology 264:16–27. https://doi.org/10.1016/j.margeo.2008.08.007

Clare M, Chaytor J, Dabson O, et al (2019) A consistent global approach for the morphometric characterization of subaqueous landslides. In: Lintern DG, Mosher D, Moscardelli L, et al. (eds) Subaqueous Mass Movements and Their Consequences: Assessing Geohazards, Environmental Implications and Economic Significance of Subaqueous Landslides. Geological Society, London, Special Publications 477, pp 455–477

Clarke SL, Hubble TC, Miao G, et al (2019) Eastern Australia's submarine landslides: implications for tsunami hazard between Jervis Bay and Fraser Island. Landslides 16:2059–2085

Collico S, Arroyo M, Urgeles R, et al (2020) Probabilistic mapping of earthquake-induced submarine landslide susceptibility in the South-West Iberian margin. Marine Geology 429:106296. https://doi.org/10.1016/j.margeo.2020.106296

Davis JC (2002) Statistics and Data Analysis in Geology, 3rd Edition. Wiley, New York

Duarte JC, Terrinha P, Rosas FM, et al (2010) Crescent-shaped morphotectonic features in the Gulf of Cadiz (offshore SW Iberia). Marine Geology 271:236–249. https://doi.org/10.1016/j.margeo.2010.02.017

Ducassou E, Fournier L, Sierro FJ, et al (2016) Origin of the large Pliocene and Pleistocene debris flows on the Algarve margin. Marine Geology 377:58–76. https://doi.org/10.1016/j.margeo.2015.08.018

Gamboa D, Alves TM (2016) Bi-modal deformation styles in confined mass-transport deposits: Examples from a salt minibasin in SE Brazil. Marine Geology 379:176–193

Gamboa D, Alves TM, Omosanya KO (2019) Style and Morphometry of Mass-Transport Deposits Across the Espírito Santo Basin (Offshore SE Brazil). In: Ogata K, Festa A, Pini GA (eds) Submarine Landslides: Subaqueous Mass Transport Deposits from Outcrops to Seismic Profiles. American Geophysical Union, pp 227–246

Gamboa D, Omira R (2021) The MAGICLAND submarine landslide database - offshore WSW Iberia. https://doi.org/10.17605/OSF.IO/S96RW

Gamboa D, Omira R, Piedade A, et al (2021a) Destructive episodes and morphological rejuvenation during the lifecycles of tectonically active seamounts: Insights from the Gorringe Bank in the NE Atlantic. Earth and Planetary Science Letters 559:116772

Gamboa D, Omira R, Terrinha P (2021b) A database of submarine landslides offshore West and Southwest Iberia. EarthArxiv. https://doi.org/10.31223/X56P52

Gamboa D, Omira R, Terrinha P (in press) A database of submarine landslides offshore West and Southwest Iberia. Sci. Data

García M, Hernández-Molina FJ, Llave E, et al (2009) Contourite erosive features caused by the Mediterranean Outflow Water in the Gulf of Cadiz: Quaternary tectonic and oceanographic implications. Marine Geology 257:24–40

Girardeau J, Cornen G, Agrinier P, et al (1998) Preliminary results of nautile dives on the Gorringe Bank (West Portugal). Comptes Rendus de l'Academie des Sciences Series IIA Earth and Planetary Science 4:247–254

Gràcia E, Dañobeitia J, Vergés J, et al (2003) Crustal architecture and tectonic evolution of the Gulf of Cadiz (SW Iberian margin) at the convergence of the Eurasian and African plates. Tectonics 22:. https://doi.org/10.1029/2001TC901045

Hampton MA, Lee HJ, Locat J (1996) Submarine Landslides. Review of Geophysics 34:33–59

Harbitz CB, Løvholt F, Bungum H (2014) Submarine landslide tsunamis: how extreme and how likely? Natural Hazards 72:1341–1374

Hernandez-Molina FJ, Llave E, Stow DAV, et al (2006) The contourite depositional system of the Gulf of Cadiz: A sedimentary model related to the bottom current activity of the Mediterranean outflow water and its interaction with the continental margin. Deep-Sea Research Part II: Topical Studies in Oceanography 53:1420–1463

Hernández-Molina FJ, Sierro FJ, Llave E, et al (2016) Evolution of the gulf of Cadiz margin and southwest Portugal contourite depositional system: Tectonic, sedimentary and paleoceanographic implications from IODP expedition 339. Marine Geology 377:7–39. https://doi.org/10.1016/j.margeo.2015.09.013

Hernandez-Molina J, Llave E, Somoza L, et al (2003) Looking for clues to paleoceanographic imprints: A diagnosis of the Gulf of Cadiz contourite depositional systems. Geology 31:19–22

Innocenti C, Battaglini L, D'Angelo S, Fiorentino A (2021) Submarine landslides: mapping the susceptibility in European seas. Quarterly Journal of Engineering Geology and Hydrogeology 54:. https://doi.org/10.1144/qjegh2020-027

Lee HJ (2009) Timing of occurrence of large submarine landslides on the Atlantic Ocean margin. Marine Geology 264:53–64. https://doi.org/10.1016/j.margeo.2008.09.009

León R, Urgeles R, Pérez-López R, et al (2020) Geological and tectonic controls on morphometrics of submarine landslides of the Spanish margins. In: Georgiopoulou A, Amy LA, Benetti S, et al. (eds) Subaqueous Mass Movements and their Consequences: Advances in Process Understanding, Monitoring and Hazard AssessmentsGeological Society, London, Special Publications. Geological Society, London, Special Publications, pp 495–513

Lo Iacono C, Gràcia E, Zaniboni F, et al (2012) Large, deepwater slope failures: implications for landslide-generated tsunamis. Geology 40:931–934

Maldonado A, Somoza L, Pallarés L (1999) The Betic orogen and the Iberian–African boundary in the Gulf of Cadiz: geological evolution (central North Atlantic). Marine Geology 155:9–43. https://doi.org/10.1016/S0025-3227(98)00139-X

Marchés E, Mulder T, Cremer M, et al (2007) Contourite drift construction influenced by capture of Mediterranean Outflow Water deep-sea current by the Portimão submarine canyon (Gulf of Cadiz, South Portugal). Marine Geology 242:247–260

Masson DG, Harbitz CB, Wynn RB, et al (2006) Submarine landslides: processes, triggers and hazard prediction. Philosophical Transactions of the Royal Society of London A: Mathematical, Physical and Engineering Sciences 364:2009–2039

McAdoo BG, Watts P (2004) Tsunami hazard from submarine landslides on the Oregon continental slope. Marine Geology 203:235–245

Medialdea T, Vegas R, Somoza L, et al (2004) Structure and evolution of the "Olistostrome" complex of the Gibraltar Arc in the Gulf of Cadiz (eastern Central Atlantic): evidence from two long seismic cross-sections. Marine Geology 209:173–198

Merle R, Jourdan F, Girardeau J (2018) Geochronology of the Tore-Madeira Rise seamounts and surrounding areas: a review. Australian Journal of Earth Sciences 65:591–605. https://doi.org/10.1080/08120099.2018.1471005

Micallef A, Berndt C, Masson DG, Stow DA (2008) Scale invariant characteristics of the Storegga Slide and implications for large-scale submarine mass movements. Marine Geology 247:46–60

Migeon S, Cattaneo A, Hassoun V, et al (2011) Morphology, distribution and origin of recent submarine landslides of the Ligurian Margin (North-western Mediterranean): some insights into geohazard assessment. Marine Geophysical Research 32:225–243

Miramontes E, Garziglia S, Sultan N, et al (2018) Morphological control of slope instability in contourites: a geotechnical approach. Landslides 15:1085–1095

Montenat, C, Guery F, Jamet M, Berthou, YB (1998) Mesozoic evolution of the Lusitanian Basin: comparison with the adjacent margin. In: Boillot, G., Winterer, L. L., et al. (eds) Proc. ODP, Sci. Results. College Station, TX (Ocean Drilling Program), pp 757–775

Moscardelli L, Wood L (2008) New classification system for mass transport complexes in offshore Trinidad. Basin Res 20:73–98

Moscardelli L, Wood L (2016) Morphometry of mass-transport deposits as a predictive tool. Geological Society of America Bulletin 128:47–80. https://doi.org/10.1130/B31221.1

Mosher DC, Shimeld JW, Hutchinson DR, Jackson HR (2016) Canadian UNCLOS extended continental shelf program seismic data holdings (2006–2011). Geological Survey of Canada, Open File 7938:

Mougenot D, Kidd RB, Mauffret A, et al (1984) Geological interpretation of combined SEABEAM, GLORIA and seismic data from Porto and Vigo Seamounts, Iberian continental margin. Mar Geophys Res 6:329–363. https://doi.org/10.1007/BF00286249

Omira R, Ramalho I, Terrinha P, et al (2016) Deep-water seamounts, a potential source of tsunami generated by landslides? The Hirondelle Seamount, NE Atlantic. Marine Geology 379:267–280

Pinheiro LM, Ivanov MK, Sautkin A, et al (2003) Mud volcanism in the Gulf of Cadiz: results from the TTR-10 cruise. Marine Geology 195:131–151. https://doi.org/10.1016/S0025-3227(02)00685-0

Pinheiro LM, Wilson RCL, Pena dos Reis R, et al (1996) The western Iberia margin: a geophysical and geological overview. In: Whitmarsh RB, Sawyer DS, Klaus A, Masson DG (eds) Proceedings of the Ocean Drilling Program Scientific Results. National Science Foundation, pp 3–26

Pope EL, Talling PJ, Urlaub M, et al (2015) Are large submarine landslides temporally random or do uncertainties in available age constraints make it impossible to tell? Marine Geology 369:19–33. http://dx.doi.org/10.1016/j.margeo.2015.07.002

Purdy GM (1975) The Eastern End of the Azores-Gibraltar Plate Boundary. Geophysical Journal International 43:973–1000. https://doi.org/10.1111/j.1365-246X.1975.tb06206.x

Roque AC, Terrinha P, Lourenço N, Abreu M (2009) Morphostructure of the Tore Seamount and evidences of recent tectonic activity (West Iberia Margin)

Siebert L (1984) Large volcanic debris avalanches: Characteristics of source areas, deposits, and associated eruptions. Journal of Volcanology and Geothermal Research 22:163–197. https://doi.org/10.1016/0377-0273(84)90002-7

Silva PF, Roque C, Drago T, et al (2020) Multidisciplinary characterization of Quaternary mass movement deposits in the Portimão Bank (Gulf of Cadiz, SW Iberia). Marine Geology 420:106086. https://doi.org/10.1016/j.margeo.2019.106086

Silva S, Terrinha P, Matias L, et al (2017) Micro-seismicity in the Gulf of Cadiz: Is there a link between micro-seismicity, high magnitude earthquakes and active faults? Tectonophysics 717:226–241

Silverman BW (1986) Density estimation for statistics and data analysis. CRC press

Stow DAV, Hernández-Molina FJ, Llave E, et al (2013) The Cadiz Contourite Channel: Sandy contourites, bedforms and dynamic current interaction. Marine Geology 343:99–114. http://dx.doi.org/10.1016/j.margeo.2013.06.013

ten Brink US, Andrews BD, Miller NC (2016) Seismicity and sedimentation rate effects on submarine slope stability. Geology 44:563–566. https://doi.org/10.1130/G37866.1

ten Brink US, Barkan R, Andrews BD, Chaytor JD (2009) Size distributions and failure initiation of submarine and subaerial landslides. Earth and Planetary Science Letters 287:31–42

ten Brink US, Geist EL (2021) On the Use of Statistical Analysis to Understand Submarine Landslide Processes and Assess Their Hazard. In: Sassa K, Mikoš M, Sassa S, et al. (eds) Understanding and Reducing Landslide Disaster Risk: Volume 1 Sendai Landslide Partnerships and Kyoto Landslide Commitment. Springer International Publishing, Cham, pp 329–341

Terrinha P, Matias L, Vicente J, et al (2009) Morphotectonics and strain partitioning at the Iberia-Africa plate boundary from multibeam and seismic reflection data. Marine Geology 267:156–174. https://doi.org/10.1016/j.margeo.2009.09.012

Terrinha P, Medialdea T, Batista L, et al (2020) Integrated thematic geological mapping of the Atlantic Margin of Iberia. Geological Society, London, Special Publications 505:SP505-2019–90. https://doi.org/10.1144/SP505-2019-90

Terrinha P, Pinheiro LM, Henriet JP, et al (2003) Tsunamigenic-seismogenic structures, neotectonics, sedimentary processes and slope instability on the southwest Portuguese Margin. Marine Geology 195:55–73

Terrinha P, Ramos A, Neres M, et al (2019) The Alpine Orogeny in the West and Southwest Iberia Margins. In: Quesada C, Oliveira J (eds) The Geology of Iberia: A Geodynamic Approach. Regional Geology Reviews. Springer, pp 487–505

Tortella D, Torne M, Pérez-Estaún A (1997) Geodynamic evolution of the eastern segment of the Azores-Gibraltar zone: the Gorringe Bank and the Gulf of Cadiz region. Marine Geophysical Researches 19:211–230

Twichell DC, Chaytor JD, ten Brink US, Buczkowski B (2009) Morphology of late Quaternary submarine landslides along the U.S. Atlantic continental margin. Marine Geology 264:4–15. https://doi.org/10.1016/j.margeo.2009.01.009

Urgeles R, Camerlenghi A (2013) Submarine landslides of the Mediterranean Sea: Trigger mechanisms, dynamics, and frequency-magnitude distribution. Journal of Geophysical Research: Earth Surface 118:2600–2618

Vázquez JT, Medialdea T, Ercilla G, et al (2008) Cenozoic deformational structures on the Galicia Bank Region (NW Iberian continental margin). Marine Geology 249:128–149. https://doi.org/10.1016/j.margeo.2007.09.014

Ward SN, Day S (2001) Cumbre Vieja volcano—potential collapse and tsunami at La Palma, Canary Islands. Geophysical Research Letters 28:3397–3400

Watson SJ, Mountjoy JJ, Crutchley GJ (2020) Tectonic and geomorphic controls on the distribution of submarine landslides across active and passive margins, eastern New Zealand. Geological Society, London, Special Publications 500:477–494. https://doi.org/10.1144/SP500-2019-165
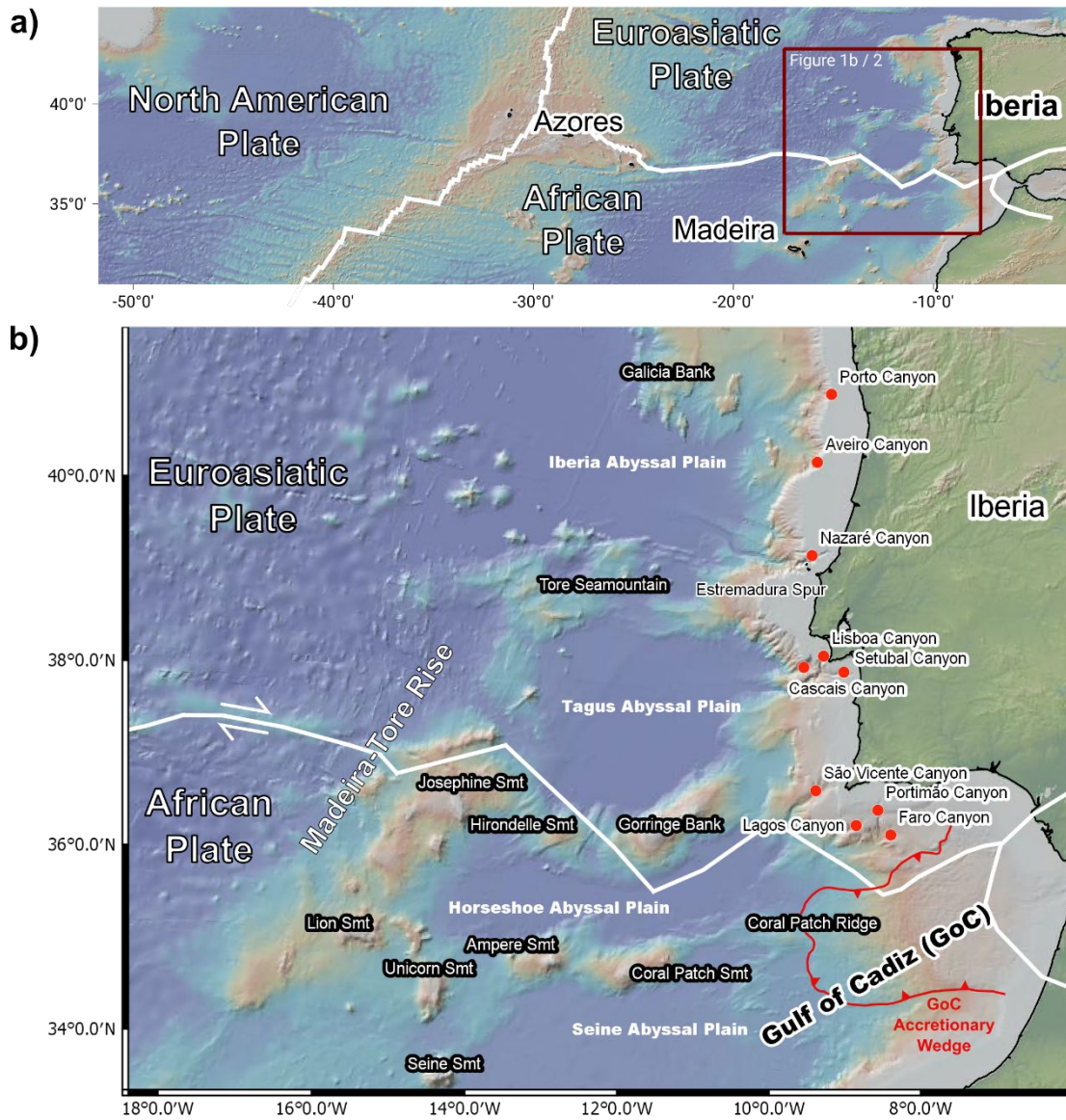
Figures

Figure 1 – a) Location of the study area limits off western and southwestern Iberia, NE Atlantic. **b)** Bathymetry of the study area highlighting main physiographic features, namely abyssal plains, seamounts and submarine canyons.
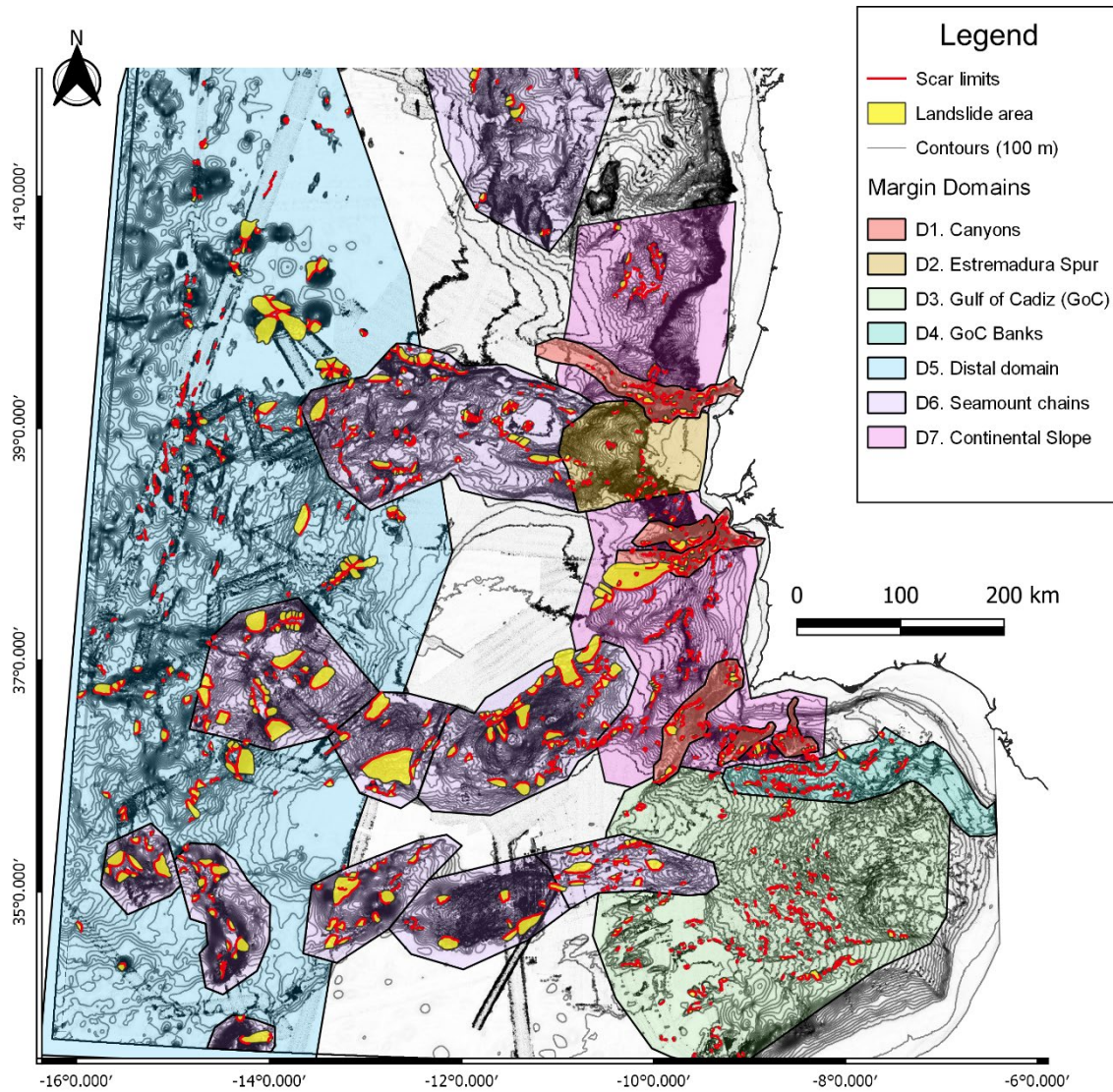
Figure 2 - Map of the landslides in the study area offshore West and Southwest Iberia. The red lines trace the limit of morphological scars identified on the EMODnet DEM. The yellow polygons adjacent to the scars depict the landslide area, but only major ones are discernible at the presented scale. Coloured polygons delimit the seven morphological domains established for this study. Contour lines were calculated from the DEM using a spacing of 100 m.
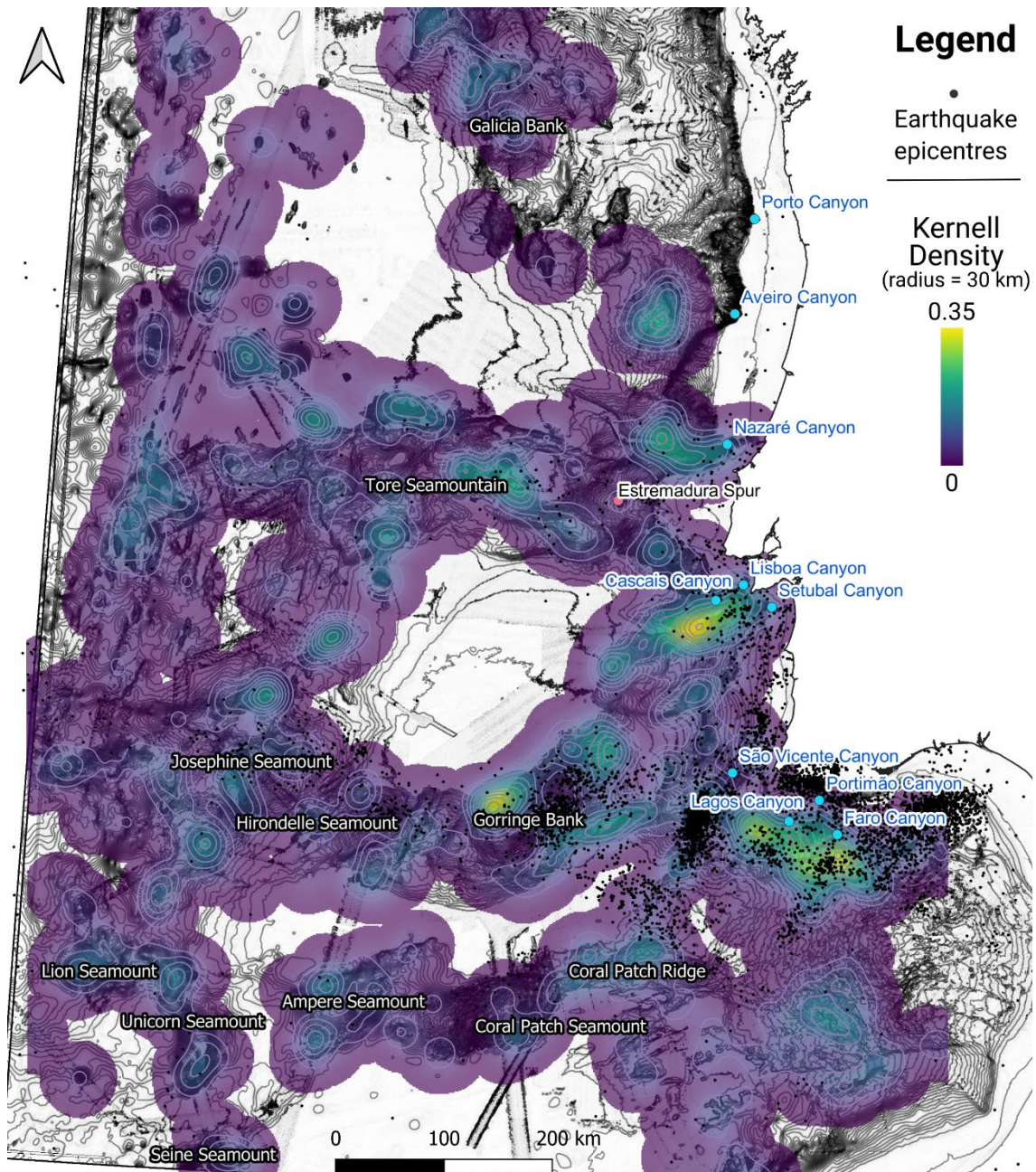
Figure 3 – Kernel Density map of submarine landslide occurrences. The main clusters are observed towards the southwest of the margin. Black dots represent epicentres of earthquakes recorded offshore.

	Domain						
	1	**2**	**3**	**4**	**5**	**6**	**7**
Nr of Points	232	38	226	123	263	437	233
Mean distance	3712.7	5894.4	4518.5	2790.4	6633	6865.5	3884
Expected distance	7681.3	6617.6	7475.1	3541.4	13749	13825	8226.8
Z	-15	-1.2	-11.37	-4.49	-16.057	-20	-15
R	0.48	0.89	0.6	0.78	0.48	0.49	0.47
Statistically significant clustering?	yes	random distrib. cannot be rejected at p<0.05	yes	yes	yes	yes	yes
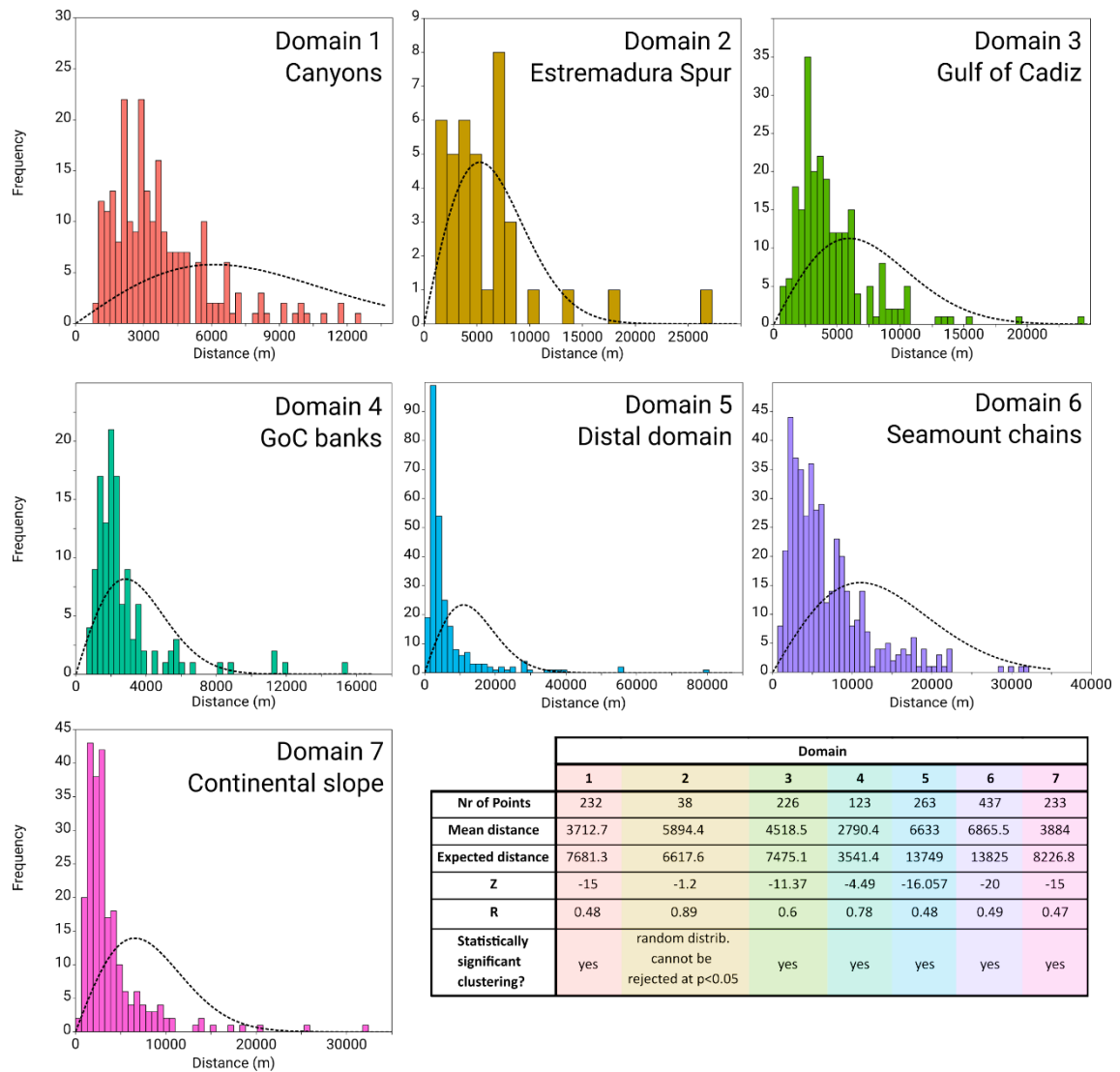
Figure 4 – Nearest-neighbour statistics for the submarine landslides within the individualised morphologic domains. The dashed curves represent the theoretical nearest-neighbour results.
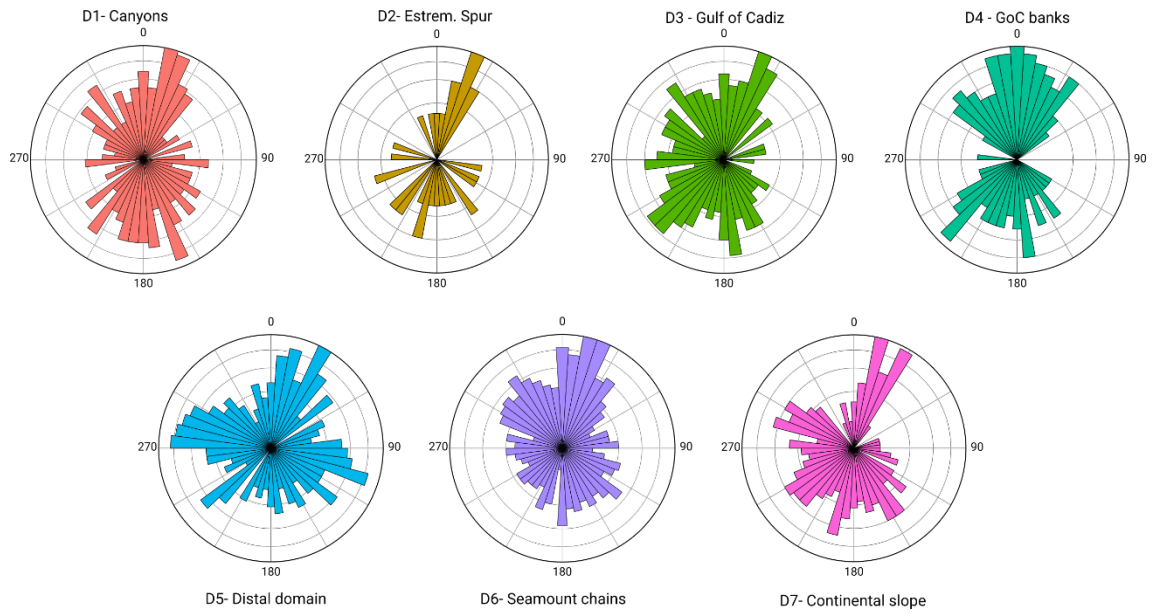
Figure 5 – Rose diagrams with the landslide flow azimuth in each morphologic domain.
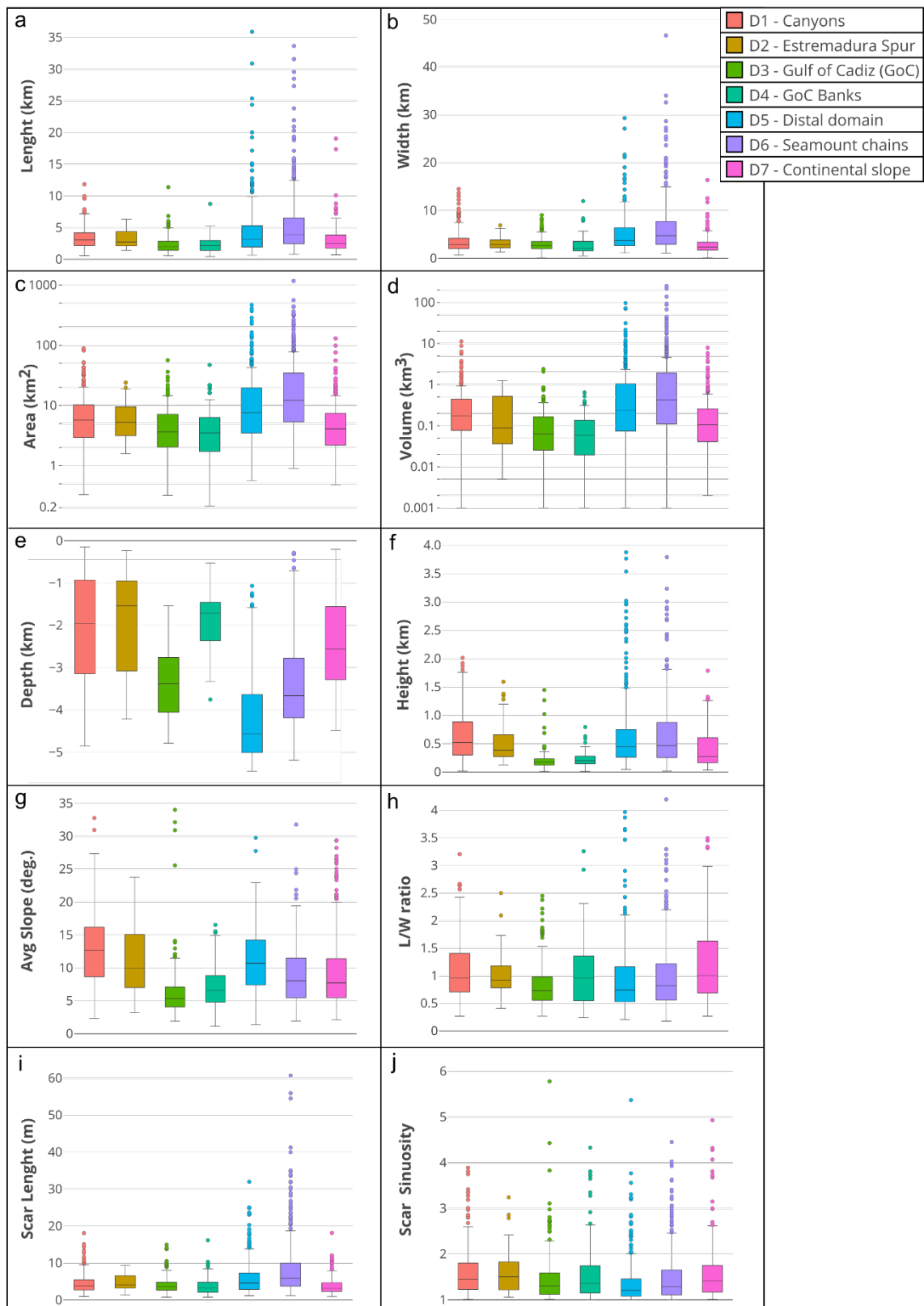
Figure 6 – Box-plots showing the range of ten morphometric parameters per each established domain.
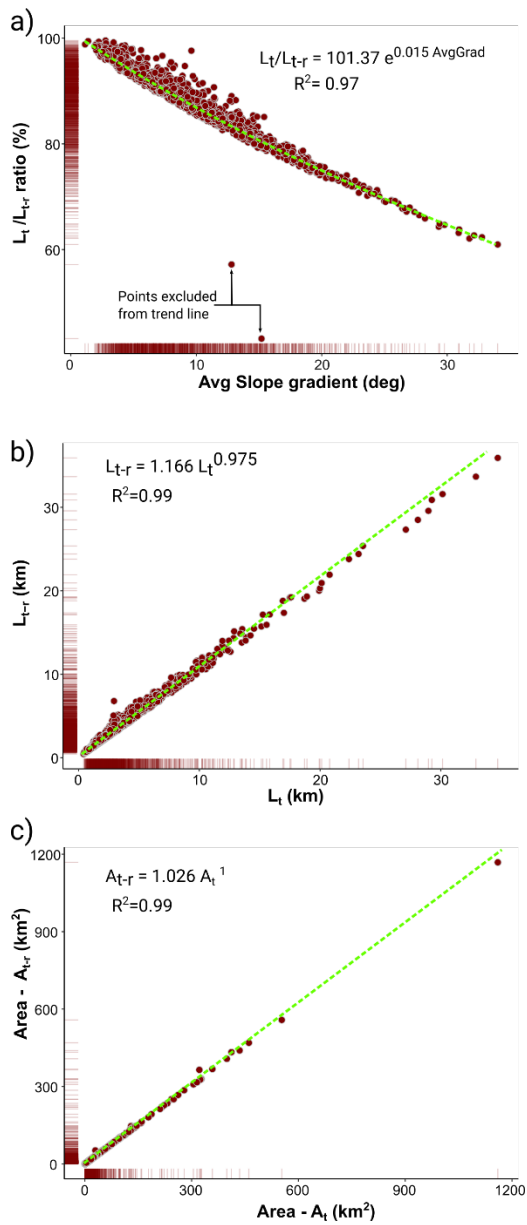
Figure 7 – a) scatter plot relating the length ratio values with the slope gradient. **b)** Relationship between the 2D planimetric length (L_t) and measured length (Lt-r) along the 3D surface. **c)** Relationship between the 2D and 3D area measurements.
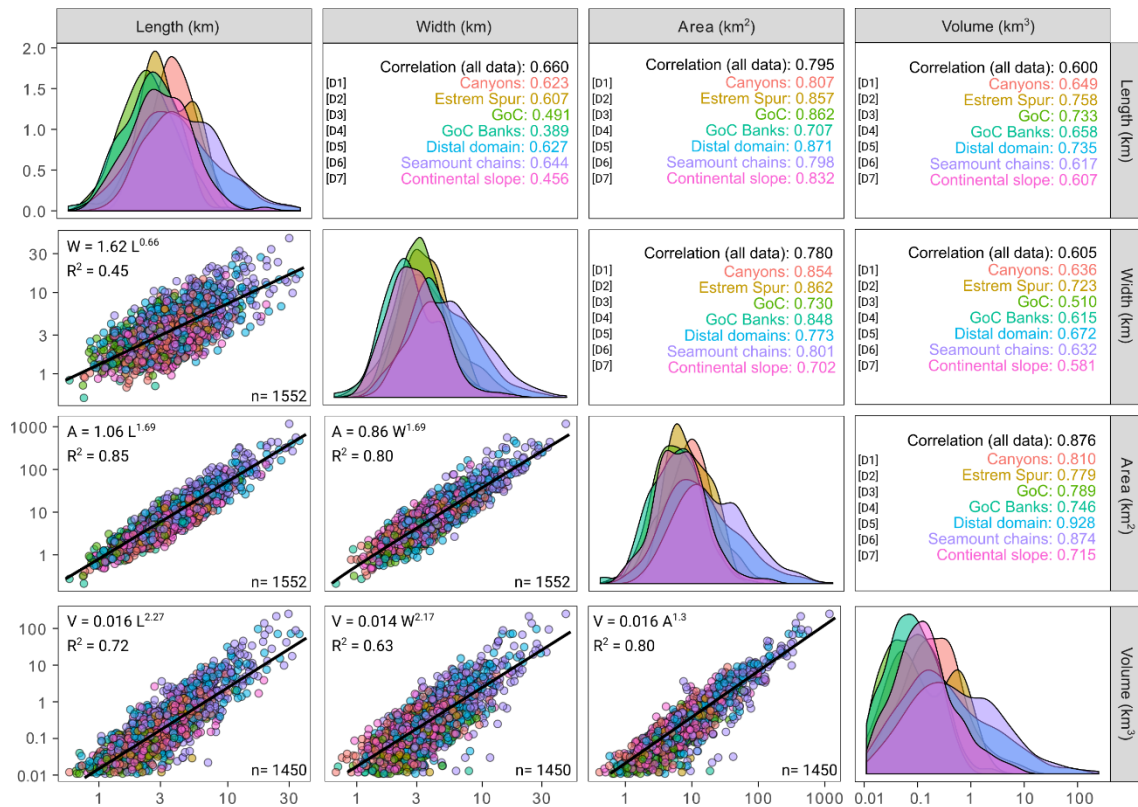
Figure 8 – Matrix plot summarising the relationships between length, width, area and volume of submarine landslides. The lower half presents parameters scatter plots, with markers coded according to their domain of occurrence. The power law relationships correspond to the full sample. The diagonal line shows the density plots of each parameter per domain. The upper half shows the Pearson correlation results between parameters.
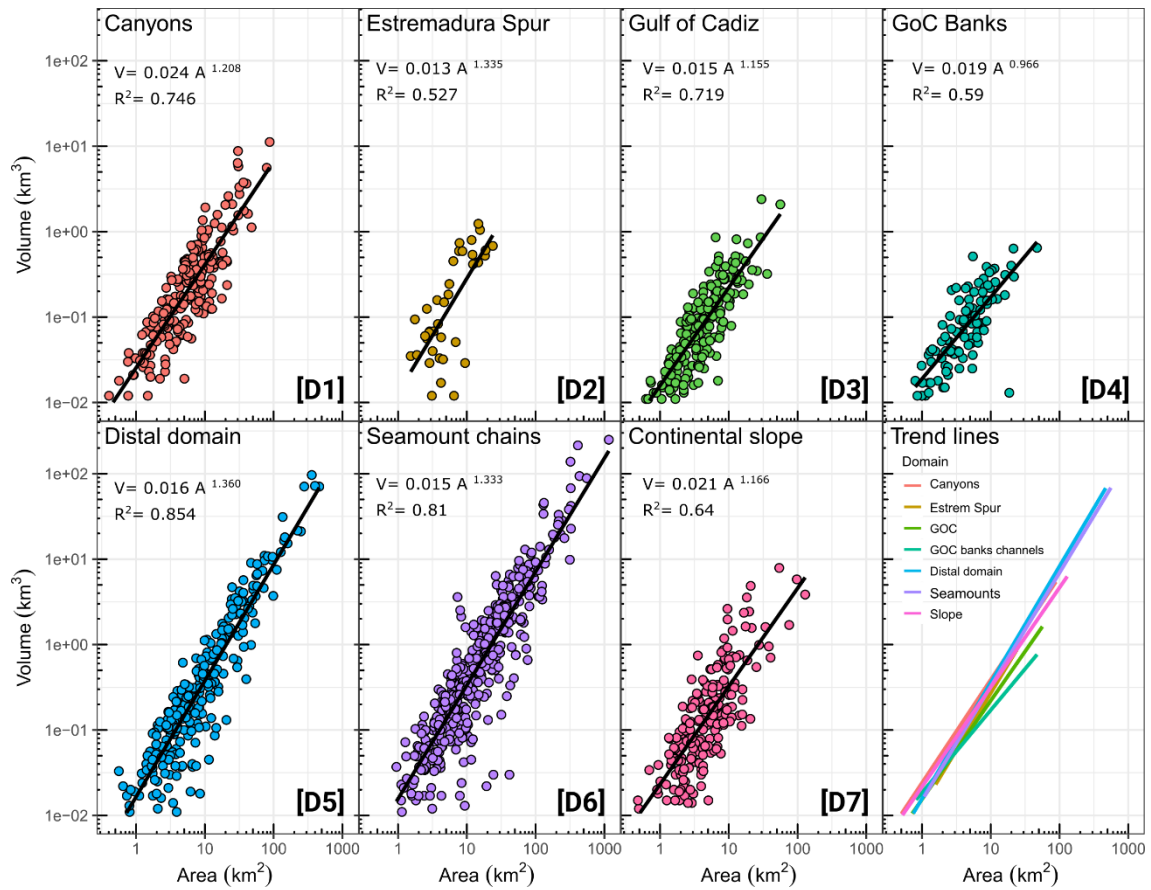
Figure 9 – Landslide area-volume relationships observed for each domain. The lower right panel compiles the diverse trendlines, colour-coded by domain.
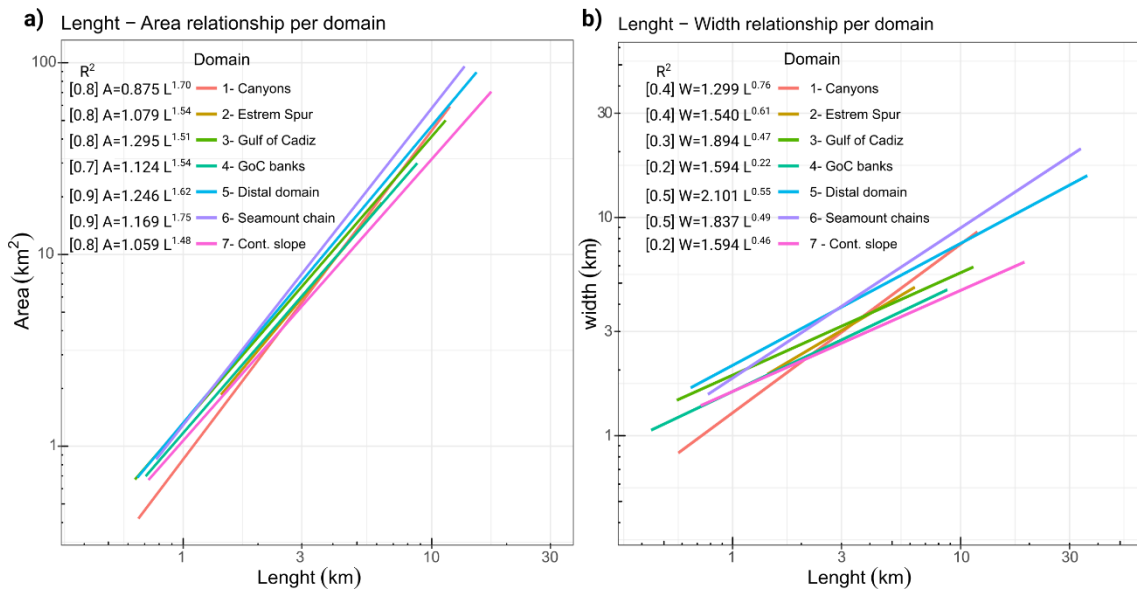
Figure 10 – Comparison of a**)** landslide length-area relationships and **b)** landslide length-width relationships. Individual coloured trendlines represent each individual domain.
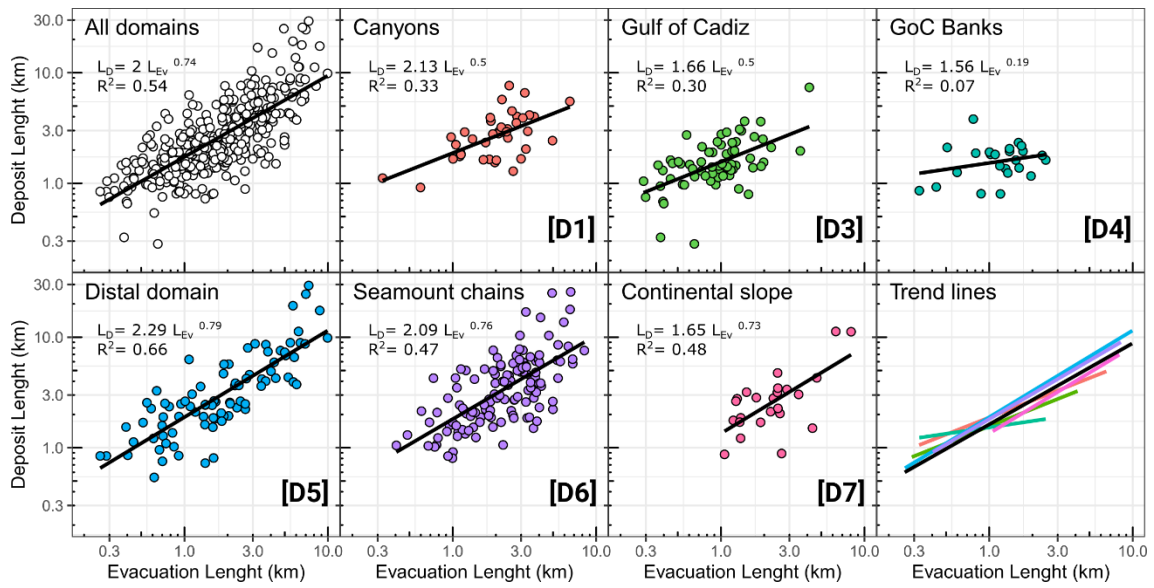
Figure 11 – Relationships between the submarine landslide evacuation length (L_{EV}) and the deposit length (L_D).
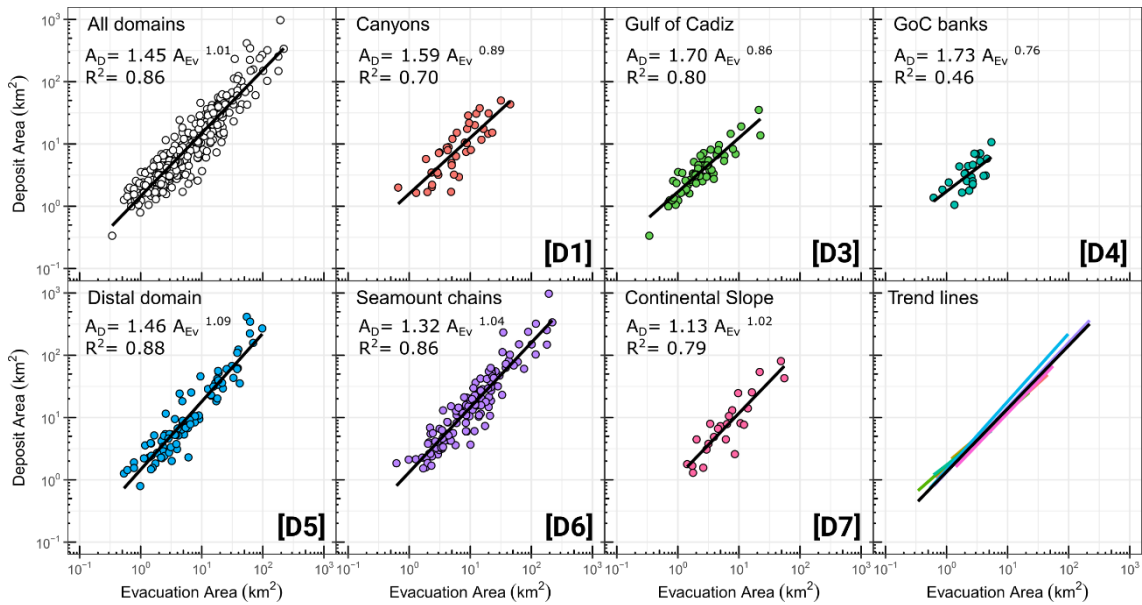
Figure 12 - Relationships between the submarine landslide evacuation area (L_{EV}) and the deposit area (L_D).